GEOSCIENCES

Sensitivity of South America Climate to Positive Extremes of Antarctic Sea Ice

CLÁUDIA K. PARISE, LUCIANO P. PEZZI, CAMILA B. CARPENEDO, FERNANDA C. VASCONCELLOS, WESLEY L. BARBOSA & LEONARDO G. DE LIMA

Abstract: Global climate change is expected to increasingly affect climate-sensitive sectors of society, such as the economy and environment, with significant impacts on water, energy, agriculture and fisheries. This is the case in South America, whose economy is highly dependent on the agricultural sector. Here, we analyzed the sensitivity of South American climate to positive extremes of Antarctic sea ice (ASI) extent and volume at continental and regional scales. Sensitivity ensemble experiments were conducted with the GFDL-CM2.1 model and compared with the ERA-Interim reanalysis dataset. The results have shown significant impacts on the seasonal regime of precipitation, air temperature and humidity in South America, such as a gradual establishment of the South Atlantic Convergence Zone, the formation of the Upper Tropospheric Cyclonic Vortex, the strengthening of Bolivian High and the presence of a low level cyclonic circulation anomaly over the South Atlantic Subtropical High region which contributed, for instance, to increased precipitation over the Southeastern Brazil. A northward shift of the Intertropical Convergence Zone was initially also a response pattern to the increased ASI. Moreover, the greatest variance of the climatic signal generated from the disturbances applied on the high southern latitudes has occurred in the interseasonal timescale (110–120 days), especially over the Brazilian Amazon and the Southeastern Brazil regions.

Key words: Southern Hemisphere Sea Ice, Antarctica-Tropics Teleconnection, South American continent, Climate Change.

INTRODUCTION

Over the last three decades (since 1978), satellite records have shown a small but significant increase in both area and volume of the Antarctic sea ice (ASI), with the two last records high in September 2013 (19.77×10^6 km^2) and October 2014 (20.11×10^6 km^2) (Cavalieri et al. 1999, Turner & Overland 2009, Holland & Kwok 2012, NOAA/NCDC 2014, Turner et al. 2015). This has been considered a climate paradox in the face of current global warming (e.g., Zhang 2007). Several mechanisms have been suggested for the increasing ASI, including ice shelf melting (Bintanja et al. 2013, Swart & Fyfe 2013), ozone depletion (Thompson & Solomon 2002, Turner et al. 2009, Goosse et al. 2009, Sigmond & Fyfe 2010, Polvani et al. 2011, Bitz & Polvani 2012), changes on climate variability modes such as the Southern Annular Mode (SAM, Thompson & Solomon 2002, Gillett et al. 2006, Thompson et al. 2011), the El Niño–Southern Oscillation (ENSO, Stammerjohn et al. 2008), the Interdecadal Pacific Oscillation (Meehl et al. 2016) and the Amundsen Sea Low (Turner et al. 2009, Meehl et al. 2016). None of these has yet yielded a consensus view of why this long-term ASI increase occurred. In the meantime, while the unexpected, decades-long overall increases

in ASI are still being puzzled out, the sea ice extent has taken a dramatic turn from relatively gradual increases to rapid decreases. The gradual increase in ASI extents reversed in the year of 2014, with subsequent rates of decline in the 2014–2017 period, far exceeding the decay rates experienced in the Arctic (Parkinson 2019). In 2017, the rapid decreases reduced the ASI extents to their lowest values in the 40-y record of satellite observations, presenting both a new yearly (2017) and monthly (February) record low.

The sea ice cover plays a fundamental role in the Earth's energy balance given its high reflectivity (albedo), its low thermal conductivity (insulating effect) and its heat and mass exchanges with the ocean and atmosphere (Budd et al. 1989). However, the impact of ASI changes on the southern atmosphere is not confined to the lower troposphere, where ocean fluxes heat it, but also extend to medium and high levels of the troposphere (e.g., Cunningham & Bonatti 2011, Raphael et al. 2011, Parise et al. 2015). In addition, the variability of ASI modulates the Equator-to-Pole temperature gradients, changing the southern heat transport and consequently the local, regional and global climate (Carpenedo et al. 2013, Parise et al. 2015, Carpenedo & Ambrizzi 2016).

Significant atmospheric disturbances, such as circulation anomalies induce the genesis of wave trains that propagate in the troposphere and transport such disturbances to remote areas, generating anomaly fields along their trajectory. Recurrent and persistent anomalous atmospheric patterns on the time scales from weeks to years when associated with anomalies generated in remote areas are defined as the preferred modes of low frequency variability or teleconnections (Cavalcanti & Ambrizzi 2009, Grimm & Ambrizzi 2009).

The sensitivity and memory of the Southern Hemisphere's coupled climate system to

increasing ASI was analyzed in Parise et al. (2015). They considered the persistence time of the ASI maxima under current climatic conditions when analyzing the Southern Hemisphere climate response. According to these authors, the disturbance of ASI maxima has resulted in a cold and fresh melting water on the surface of the Southern Ocean, which starts to represent the memory of the ocean under a sudden anomaly applied on the ASI field. The authors found that the mechanism responsible for restoring the climatic equilibrium state is triggered by a dual timescale mechanism, which is initiated by the sea ice isolation effect and the resulting melting freshwater pulse (the rapid response) and restored by the heat stored in the subsurface layers of the Southern Ocean, as the sea ice-resulting fresh and cold surface water is advected to the lower latitudes (the slow response).

Global climate change is expected to significantly affect economic sectors that are highly sensitive to climate, such as agriculture, water, energy and fisheries (Mendelsohn et al. 2006), as is the case in South America, whose economy is highly dependent on the agriculture sector. The tremendous territorial extension of South America covering an extensive latitudinal range and its various forms of topographic relief allow the formation, development and action of different atmospheric systems that characterize accentuated climate heterogeneity to this continent. Cold frontal systems, cyclones and anticyclones coming from Antarctica move preferentially to the east-northeast, with a large contribution of the air masses of Western and Eastern Antarctic Peninsula (Jones & Simmonds 1993, Sinclair 1994, Simmonds et al. 2003, Carpenedo 2012, Turner et al. 2020).

Based on the same numerical experiments performed by Parise (2014), whose details are the next section, this study aimed to investigate

the sensitivity of the South American climate to positive extremes of ASI, in area and volume, at continental and regional scales. The Pole-Equator teleconnection mechanisms associated with the high latitude climatic signal are also evaluated.

NUMERICAL SIMULATIONS AND CLIMATE DATA

We analyzed the changes found over the South America continent in response to ASI maxima looking at the seasonality of main atmospheric systems acting in each season, with the focus on the region with the highest biases in precipitation, air temperature, humidity and winds.

The climate data used in this study originated from two ensemble simulations carried out with the National Oceanic and Atmospheric Administration/Geophysical Fluid Dynamics Laboratory (NOAA/GFDL) Coupled Model (CM2.1 version). This model was also used in the generation of a set of experiments on climate change for the Fourth Assessment Report (AR4) of the Intergovernmental Panel on Climate Change (IPCC), published in 2007. The CM2.1 model has four components (atmosphere, continent, ocean and sea ice) that interact with each other through the Flexible Modeling System (Delworth et al. 2006). The numerical experiments used here were configured to explore the potential impacts of increasing melting water fluxes from the ASI on the dynamics of the Southern Ocean, as already shown by Parise et al. (2015), and also to understand how this signal propagates meridionally and finally, modulates the South American climate. The simulations were carried out for a period of 10 years (from July 2020 to June 2030) under two different conditions of ASI, a climatological condition hereafter named as *layerctl* experiment and a positive maximum

condition hereafter named as *layermax* experiment (Table I).

The initial conditions for the *layerctl* were generated from restarts files for the months of July, August and September (the two months preceding and the month that presents, climatologically, the largest sea ice cover in the Southern Hemisphere) of a coupled simulation integrated for 10 years (totaling 30 members). The maximum concentration of ASI, in turn, was calculated from the Met Office Hadley Center (HadISST1) data set (1870–2008) (Rayner et al. 2003), while the maximum thickness was calculated from a monthly climatology provided by the GFDL (1979–1996) (Taylor et al. 2000). Both conditions (area and volume) represented the maximum value of sea ice in the time series for each major point, regardless of when it occurred in time. Both ensemble simulations were initialized from a 30-year spin-up model round (1990–2020) (Table I). More details about configuration and performance of the sensitivity experiments used in the present study can be seen in Parise (2014) and Parise et al. (2015). In this study, only the first 4 years (2020–2024) of model integration were evaluated because they represent the period with the largest positive ASI differences (Parise et al. 2015) (Table I).

The southern troposphere wind dataset used to validate the CM2.1 model simulations are derived from the European Center for Medium-Range Weather Forecasts (ECMWF) ERA-Interim Reanalysis (Dee et al. 2011), from 1979 to present. For precipitation comparisons, the Global Precipitation Climatology Project (GPCP) monthly precipitation dataset (Adler et al. 2003) is used, which combines observations and satellite precipitation data into 2.5° in longitude and 2.5° in latitude global grid. Here, only the last 4 years available to date (2017–2020) were compared to the first 4 years of the control's ensemble experiments (Table I).

Table I. Schematic table with basic information on the sensitivity experiments performed with the CM2.1 model and used in this study, as a complement to that presented by Parise et al. (2015).

	layerctl	*layermax*
Horizontal and vertical resolution of the atmospheric component	2.5° in longitude and 2° in latitude, with 24 vertical hybrid sigma-pressure levels	
Model spin-up	a short (1 year) uncoupled simulation, with only the ocean and sea ice models, followed by a long (30 years) fully coupled integration, from 1990 to 2020	
Initial conditions for ASI concentration (%)	a control model integration of 10 years forward from the spinup, where the restarts conditions for each July–August–September (JAS) were used	Met Office Hadley Center dataset, from 1870 to 2008 (Rayner et al. 2003)
Initial conditions for ASI thickness (m)		GFDL monthly climatology from 1979 to 1996 (Taylor et al. 2000)
Running-period (Parise 2014)	10 years, from July 2020 to June 2030	
Running-period analyzed in the presente study	the first 4 years, from July 2020 to June 2024, as it represents the positive ASI phase (Parise et al. 2015)	

METHODS

The South American climate analysis was carried out through the identification of the main atmospheric systems that determine the heterogeneity of the precipitation regime in this continent in each season of the year. The results of the *layerctl* ensemble simulation were discussed with what is known in the literature in terms of atmospheric systems acting at low and high levels of the troposphere through comparisons with the ERA-Interim reanalysis data. The impacts on the South American climate resulting from the increase in ASI were analyzed seasonally (SON, DJF, MAM and JJA) and for each year of model simulation (t_1, t_2, t_3, and t_4), in order to determine not only the degree of sensitivity but also the response time of this continent.

However, studies of weather and climate conditions and their local and remote agents must consider the large latitudinal extent and the various forms of the South American topography, which allows the development and performance of several atmospheric systems, reflecting in a climate heterogeneity (space-time) and a very regionalized precipitation regime. Thus, the climate analysis of changes over South America resulting from the increased ASI was performed spatially, in the domain of the continent, and spectrally, through time series for six regions (R1 to R6) with distinct climate regime (Ratisbona 1976, Pezzi & Kayano 2008), namely: Northwestern South America (R1), Brazilian Amazon (R2), Northeast Brazil (R3), South Northeast Brazil (R4), Southeastern Brazil (R5) and Southern Brazil (R6) (Figure 1).

The spatial and seasonal variability was assessed regionally based on atmospheric fields of air temperature (°C) and specific humidity (kg_{water}/kg_{air}) at 850 hPa, accumulated precipitation rate (mm season^{-1}) and associated circulation at 850 hPa and 200 hPa. The validation (Supplementary Material - Figures S1-S4) of the control experiment over the South America continent was made through the interpolation of the model data to the ERA-Interim grid. The
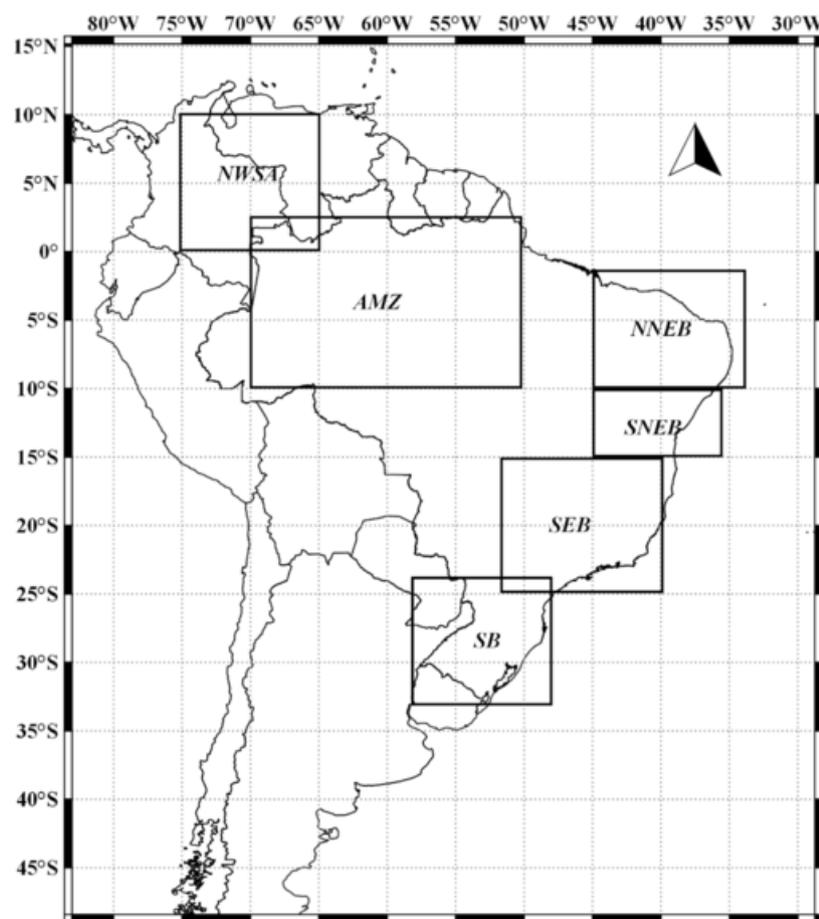
Figure 1. Area of the six regions with heterogeneous climate in Sotuh America analyzed in this study: **R1 – Northwest of South America, R2: Brazilian Amazon, R3: North of Northeast Brazil, R4: South of Northeast Brazil, R5: Southeast Brazil and R6: South Brazil. As suggested in Pezzi & Kayano (2008).**

timescales (or periodicities) of the climatic signal generated from the ASI anomalies were extracted from each of the six regions with heterogeneous climate regime (R1 to R6) through the spectral analysis of wavelet transform (Pezzi & Kayano 2008, Veleda et al. 2012).

RESULTS

Sensitivity of South American climate to Antarctic sea ice extremes

The main impacts from positive ASI extremes on the climate of South America are here analyzed through the changes in the 925 hPa atmospheric temperature (°C) and specific humidity, the accumulated precipitation rate (mm season^{-1}) and the associated wind (ms^{-1}) at lower (925 hPa) and upper (200 hPa) levels. This part of the study focuses on the seasonal variability of the *layerctl* ensemble integration with the analysis performed separately for each year of integration (t_1, t_2, t_3 and t_4) in order to avoid loss of information arising from the 4-year average. The major changes are highlighted below, not necessarily in the temporal order (from t_1 to t_4) but according to the year with the largest impacts.

Spring

The impact of the ASI extremes on the South American climate during the spring (SON) are shown in Figure 2. In the fourth year (t_4), enhanced precipitation (80 mm, which represents ~8% more) is found in an orientated
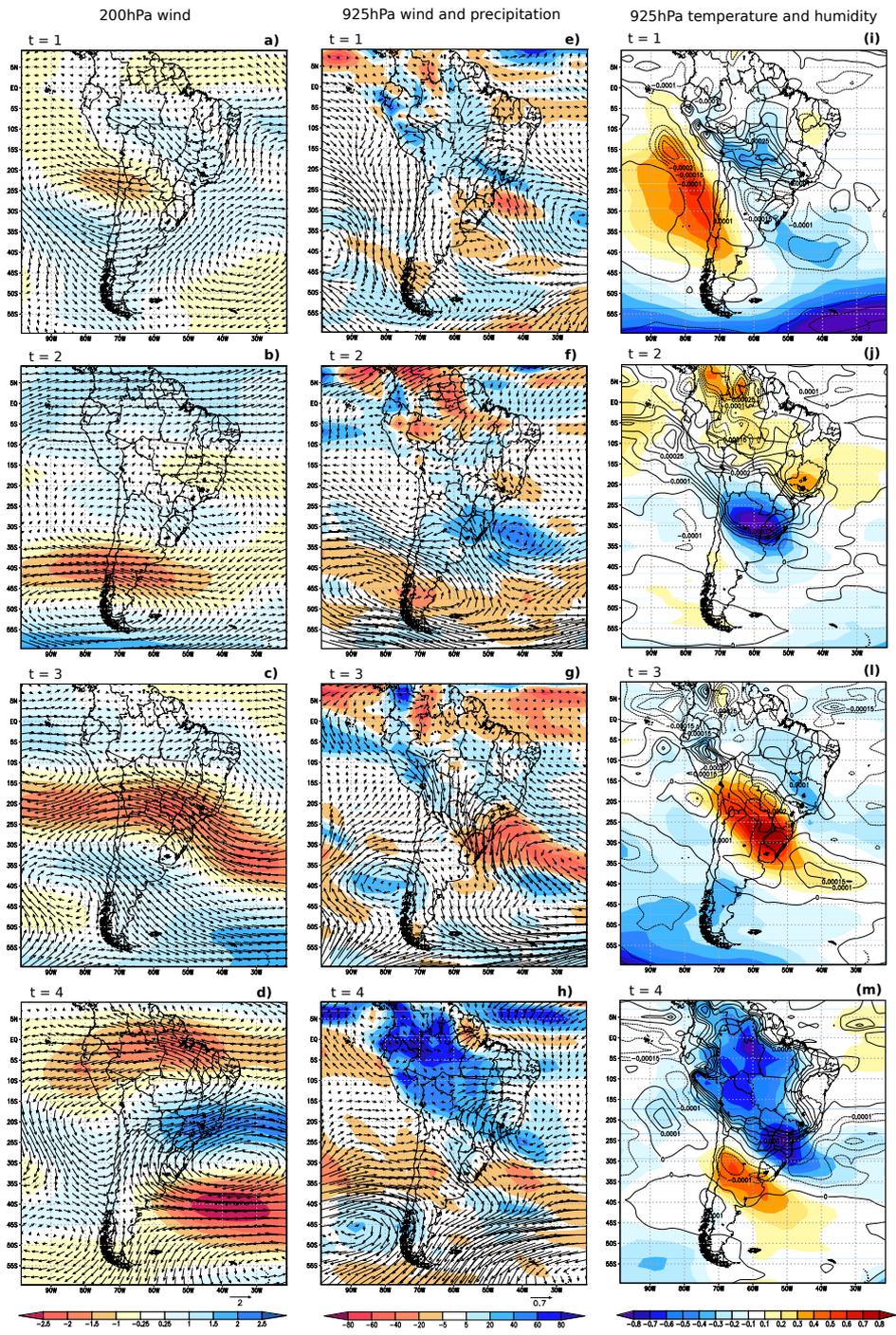
Figure 2. Left column: Changes in the 200hPa zonal wind magnitude and vector (m s⁻¹); **Middle column:** Changes in the accumulated precipitation rate (coloured shades, mm season⁻¹) and 925hPa wind (vectors, m s⁻¹); and **Right column:** Changes in the air temperature (coloured shades, in °C,) and 925hPa specific humidity (contour lines, in kg_{water}/kg_{air},); The changes were obtained from *layermax-layerctl* diferences in each year of simulation (t_1, t_2, t_3, and t_4) during the spring (SON).

northwest-southeast convective band originating from the Amazon basin (Equator/ Peru) extending towards Southeastern Brazil (Figure 2h). This characterizes a South Atlantic Convergence Zone (SACZ) circulation pattern (Pezzi et al. 2022). The SACZ and convective activity in the Amazon basin are the main components of the South American monsoon system (Zhou & Lau 1998). Associated with this, an increase in the specific humidity (~0.0003 kg_{air}/kg_{water}) and a reduction in the 925 hPa air temperature (~0.8°C colder) (Figure 2m) are observed in association

with a cyclonic circulation at low levels over the adjacent oceanic region, the Southeastern Brazil (Figure 2h). Essentially, negative differences in air temperature (blue shadings) and positive differences of specific humidity (solid contours) at 925 hPa (Figure 2i-m) are associated with positive differences of precipitation (blue shadings) (Figure 2e-h). Moreover, the subtropical jet over the Atlantic Ocean basin is weakened in its climatological position (35°S) and enhanced further north in the latitudinal band of 15°S–25°S (Figure 2d). Also, a strengthening of the Bolivian High is clearly observed in t_4. Likewise, over Southeastern South America (SESA), there are positive anomalies of humidity and negative anomalies of air temperature (Figure 2m) associated with a cyclonic circulation at low levels (Figure 2h). While in t_4, a SACZ pattern is established, resulting in less precipitation over the SEAS region, in t_2, the response was opposite, which means, the SACZ is undone and precipitation is increased over SEAS (Figure 2f and 2j). This out-of-phase response is also observed through alternating westerly and easterly winds at lower levels (Figure 2b and 2d), a typical precipitation pattern of the warmer semester of the South American monsoon system (Jones & Carvalho 2002). During the third year of simulation (t_3), differences in air temperature, specific humidity and precipitation over SEAS are also observed. The ASI extremes reduce the precipitation over the South and coast of Southeastern Brazil (Figure 2g) and raise the air temperature over the SESA (Figure 2l). These are associated with an anticyclonic circulation at lower levels (Figure 2g), indicating the performance of an atmospheric blocking over the Southwestern Atlantic Ocean (Manta et al. 2018). Additionally, the zonal wind magnitude at 200 hPa is reduced (red shading and easterly wind anomalies) over the latitudinal band of 15°S–30°S and is enhanced (light blue shading

and westerly wind anomalies) over the south of South America (Figure 2c). This indicates a weakening (strengthening) of the subtropical jet (polar jet), respectively, which has carried out the precipitation southward. These results reinforce the conducting of the positive phase of SAM (Thompson & Wallace 2000, Parise et al. 2015) directly related to increased ASI extent (Pezza et al. 2012, Parise et al. 2015). Even during the third year, the north-northwest wind anomalies are observed at low levels extending over South America from the Northwestern Amazon towards the East-Southeast of Brazil (Figure 2g). These changes in the mean circulation were related to the performance of the low level jet east of Andes that brings humidity (Figure 2l) and precipitation (Figure 2g) to Peru. This instability condition does not reach the south-southeast regions of Brazil because the anticyclonic circulation at the low levels found there (Figure 2c).

Summer

The impacts of the ASI extremes on the South American climate during the summer (DJF) are shown in Figure 3. For this season, a gradual (t_1, t_2, t_3 and t_4) decrease in the 925 hPa air temperature is observed, with negative differences appearing first in a northwest-southeast oriented band over the south and central regions of Argentina (t_1, Figure 3i) and sequentially reaching the south and southeast regions of Brazil (t_2, Figure 3j), the north of Argentina (t_3, Figure 3l) and the west, central and east of Brazil (t_4, Figure 3m). In the second year (t_2), a cyclonic circulation begins to develop at low levels over Southeastern Brazil, contributing to wind convergence and increased precipitation (Figure 3f). Also, warm and dry biases are found in the north and northeast Brazil at t_2 (Figure 3j) and north of Argentina at t_4 (Figure 3m), both associated with reduced precipitation (Figure 6f and Figure 6h, respectively). In t_3, the cyclonic center over the
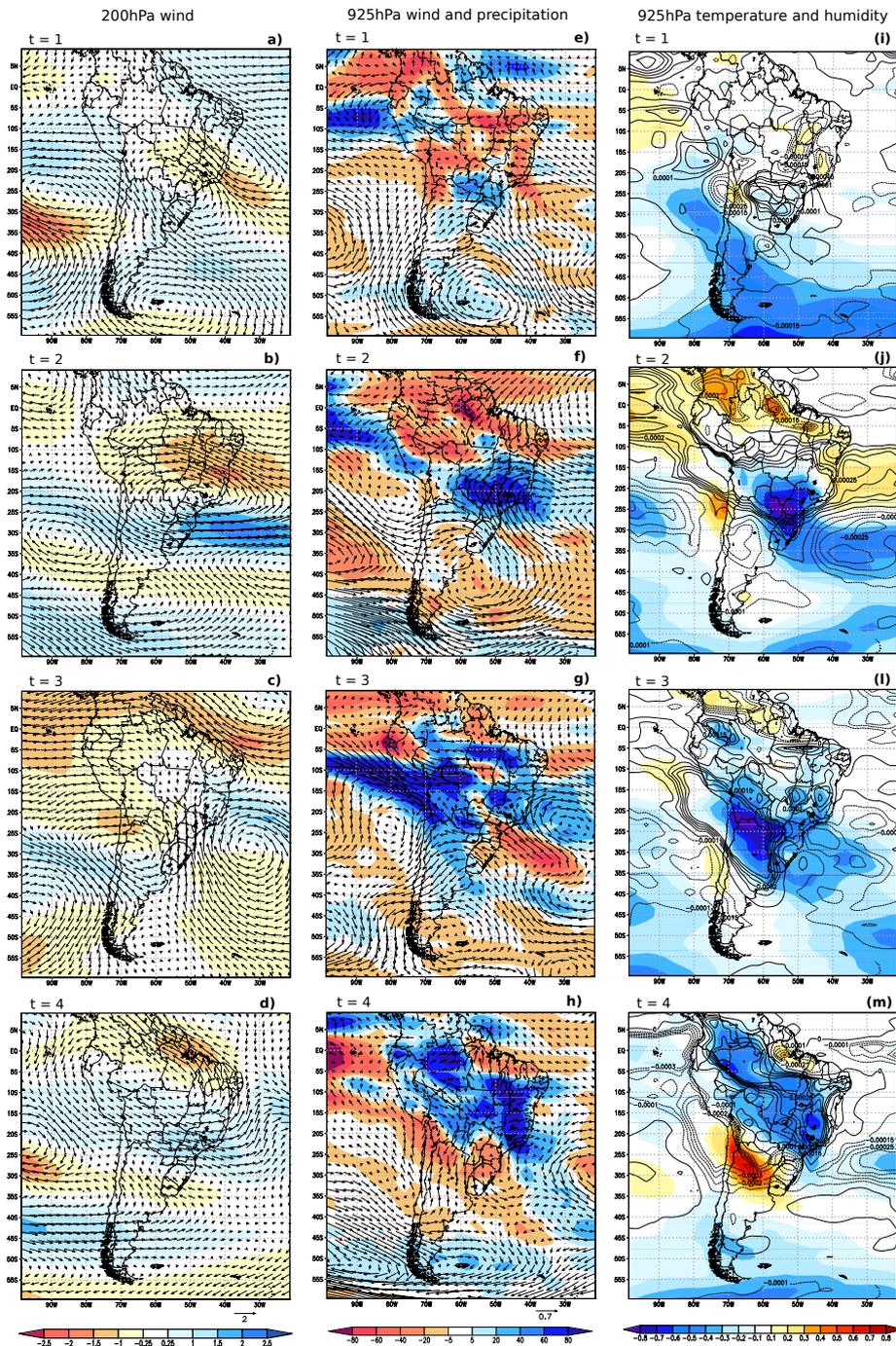
Figure 3. Left column: Changes in the 200hPa zonal wind magnitude and vector (m s^{-1}); **Middle column:** Changes in the accumulated precipitation rate (coloured shades, mm season^{-1}) and 925hPa wind (vectors, m s^{-1}); and **Right column:** Changes in the air temperature (coloured shades, in °C,) and 925hPa specific humidity (contour lines, in kg$_{water}$/kg$_{air}$); The changes were obtained from *layermax-layerctl* diferences in each year of simulation (t$_1$, t$_2$, t$_3$, and t$_4$) during the summer (DJF).

adjacent oceanic region moves further north, leading to the positive precipitation anomalies also moving northward (Figure 3g). These wind anomalies then extend towards the upper levels (see the cyclonic circulation over the Atlantic Ocean in Figure 3c). It is possible to observe that this upper level cyclonic center (~32°W and 27°S) keeps moving northward up to the point of intensifying the Brazilian Northeast Though during the t$_4$ (Figure 3d). Associated with that, there was an intensification of the Bolivian High which contributed for the establishment of a SACZ pattern. According to Kousky & Gan (1981), when frontal systems from mid-latitudes

move northward, the air convection may act to intensify the ridge at upper levels. As a consequence, the trough upstream of the ridge is amplified, favoring the Upper Tropospheric Cyclonic Vortex (UTCV). As this cyclonic vortex has a cold core, the air subsides at its center and rises at its periphery, favoring the convection and the existence of clouds only at its periphery, as observed in Figure 3h. That response suggests that positive ASI extreme conditions contribute to the genesis of the UTCV. Moreover, strengthening of an upper level anticyclonic center is observed at t_2 (Figure 3b), although slightly shifted to the east in relation to the climatological position of Bolivian High (Lenters & Cook 1997), acting as another factor to the precipitation formation over the region. So, during the southern summer, the increased precipitation over most parts of Brazil (Figure 3h) is facilitated by an increase in humidity and a decrease in air temperature (Figure 3m) caused by a gradual establishment of a SACZ pattern and by the Bolivian High and Brazilian Northeast Though strengthening at upper levels (Figure 3d).

Autumn

The impacts of the ASI positive extremes over the South American climate during the autumn (MAM) are based in Figure 4. The ASI maxima could modify the Intertropical Convergence Zone (ITCZ) either weakening (Figure 4e) or intensifying (Figures 4f and 4h) it. While the precipitation and humidity are generally intensified over the ICTZ, an opposite response is again observed at t_3. Looking at the air temperature changes, it was possible to notice a dipole-like pattern, with positive differences over the central region of Brazil as well as negative differences over its boundary region with Argentina in the first two years (Figures 4i and 4j). In the third year, however, the air temperature dipole shows

an opposite signal (Figure 4l). Associated with the negative air temperature anomalies over Southern Brazil at t_1, enhanced precipitation and a low level cyclonic circulation over the adjacent oceanic region is observed (Figure 4e), which extends towards the upper levels (Figure 4a). During the following year (t_2), the negative differences of air temperature over Southern Brazil move southwards, and the positive differences over the central region of Brazil are intensified (Figure 4j). This is associated with the development of an anticyclonic circulation at upper levels (Figure 4j), also responsible for the negative precipitation differences throughout the central South America from the Pacific to the Atlantic coast (Figure 4f). The positive air temperature and negative humidity differences over Southern Brazil at t_3 indicates that there are not cold fronts acting there. The anticyclonic circulation at upper levels found at t_2 is again observed at t_3, although shifted slightly southward, over Brazil-Paraguay-Argentina (Figure 4c). In the t_4, the ASI extremes cause increased precipitation and humidity over the Southwestern and Southeastern Brazil and over Paraguay, Bolivia, Northern Chile, Southern Peru and Eastern Pacific region, associated with northwest wind differences converging from the Pacific Ocean (Figures 3h and 3m).

Winter

The impacts of the ASI extremes on the South American climate during the southern winter (JJA) are discussed based on Figure 5. The results for winter are shown only for the first three years (t_1, t_2 and t_3), once the ensemble model integrations started in July and this month and the following (August) were discarded of analysis as this does not constitute a season (or three months period) representative of winter. So, the first winter refers to the year 2021 instead of 2020 (Parise 2014). In the first year, positive air
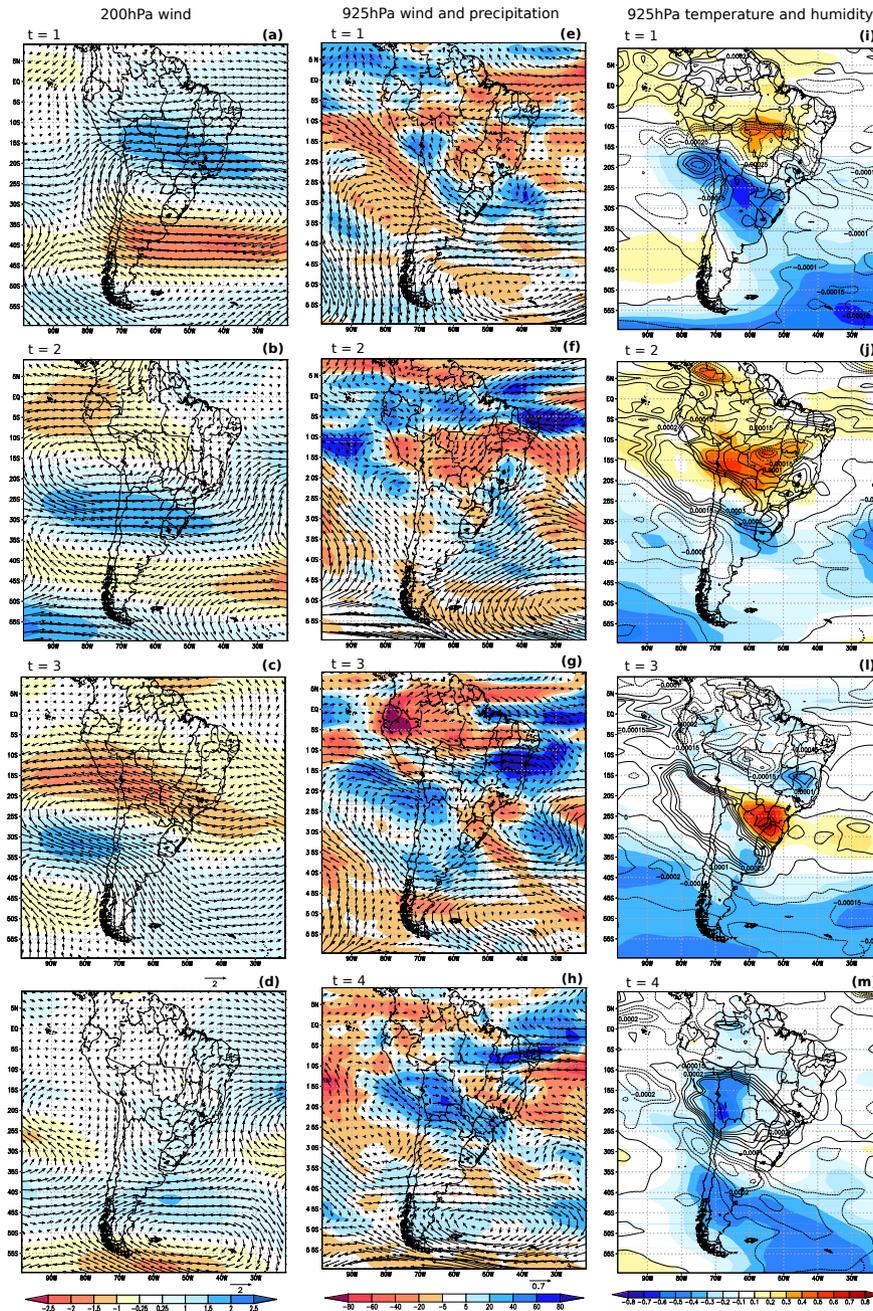
Figure 4. Left column: Changes in the 200hPa zonal wind magnitude and vector (m s^{-1}); **Middle column:** Changes in the accumulated precipitation rate (coloured shades, mm season^{-1}) and 925hPa wind (vectors, m s^{-1}); and **Right column:** Changes in the air temperature (coloured shades, in °C,) and 925hPa specific humidity (contour lines, in kg$_{water}$/kg$_{air}$); The changes were obtained from *layermax-layerctl* diferences in each year of simulation (t$_1$, t$_2$, t$_3$, and t$_4$) during the autumn (MAM).

temperature differences were found along the western coast of South America (Figure 5g). Over the Equatorial Atlantic, a strengthening of the SE trade winds and a reduction in precipitation were observed (Figure 5d) during t$_1$, indicating a northward shift of the ITCZ. In the following years, the trade winds are reserved, coming from the N-NW (Figures 5e and 5f). Also, an anomalous cyclonic circulation is formed over the Southwestern Atlantic Ocean and then moves northeast of the region. At its rear, a strong anticyclonic anomaly has carried out cold and moisture air masses from Antarctica. As a consequence, decreased air temperature and increased air humidity are found over the SESA (Figure 5h) and then extending both towards the northwest and southeast (Figure 5i). The numerical experiments performed here
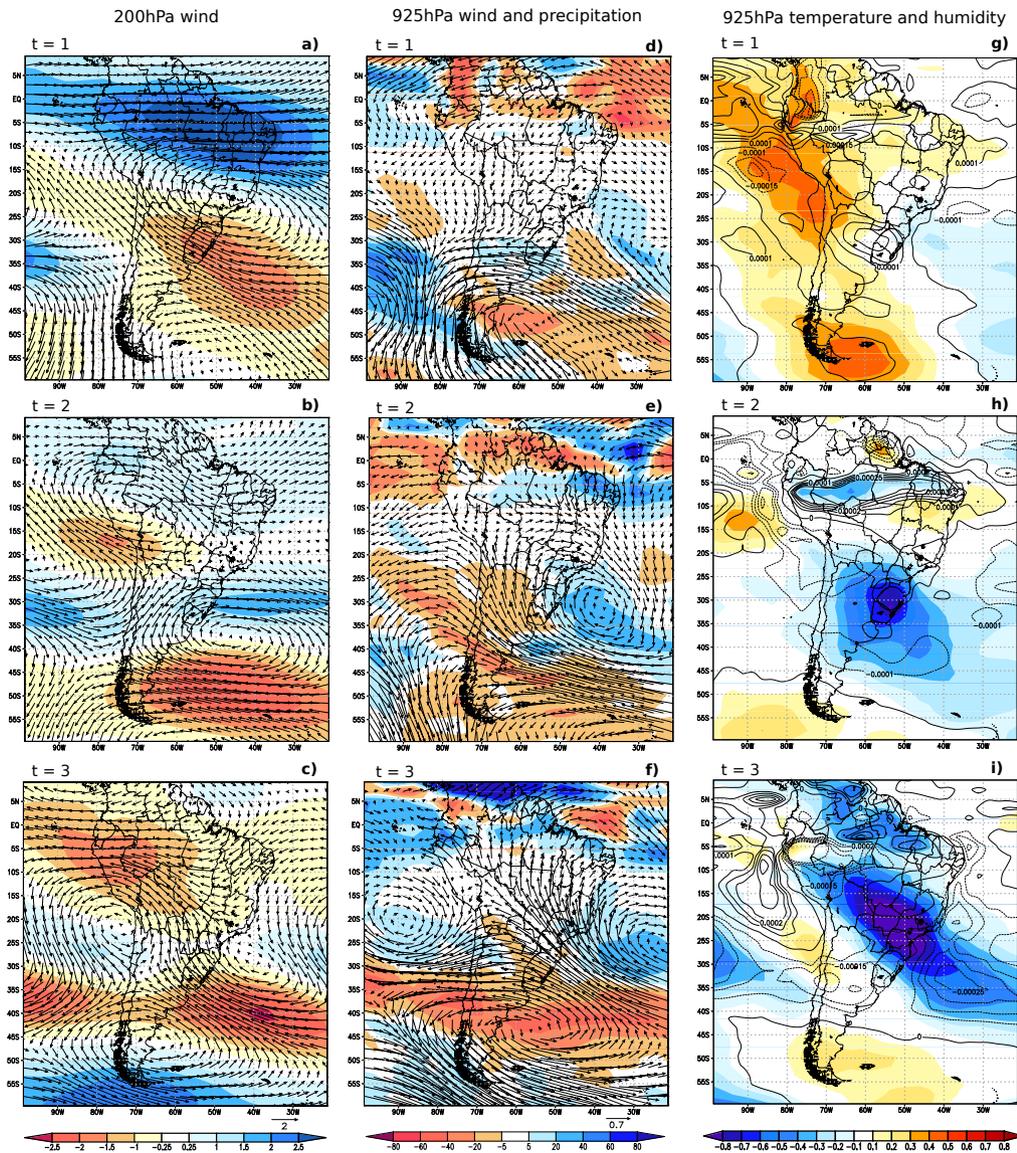
Figure 5. Left column: Changes in the 200hPa zonal wind magnitude and vector (m s^{-1}); **Middle column:** Changes in the accumulated precipitation rate (coloured shades, mm season^{-1}) and 925hPa wind (vectors, m s^{-1}); and **Right column:** Changes in the air temperature (coloured shades, in °C,) and 925hPa specific humidity (contour lines, in kg$_{water}$/kg$_{air}$); The changes were obtained from *layermax-layerctl* diferences in each year of simulation (t$_1$, t$_2$, t$_3$, and t$_4$) during the winter (JJA).

show that ASI positive extremes can impact the precipitation regime over the Southern South America (SSA), including Uruguay, Argentina and Southeastern Brazil. A northwest-southeast oriented band of reduced precipitation over this region is observed, which is associated with an anticyclonic circulation at low levels at east of Argentina (Figures 4e and 4f) and extends to the upper levels (Figures 8b and 8c), indicating a weakening of subtropical jet and poleward shift of polar jet. Furthermore, the enhanced baroclinicity over mid-latitudes and increased track density over higher latitudes discussed in

Parise (2014) may have contributed to reduce the precipitation over the subtropical region. Reduced precipitation over SSA (Figure 5d) and over Southern Brazil (Figure 5f) is found sequentially in time (t$_1$, t$_2$, t$_3$, t$_4$). The increased precipitation over Southern and Southeastern Brazil has been associated with a cyclonic circulation over the Southwestern Atlantic Ocean. This anomaly extends baroclinically from the lower to upper levels (Figure 5a-f). Climatologically, the South Pacific Subtropical High (SPSH) is located further north during the winter (JJA), causing the westerlies to be

adiabatically cooled and forced down when crossing the Andes, favoring the precipitation over the SESA. Our results indicate that both South Atlantic Subtropical High (SASH) and SPSH have weakened in the third year of model integration (t_3), to the point of allowing the northward shift of the anticyclonic anomaly that propagates from Antarctica. Moreover, the transient eddies (i.e., cold fronts and extratropical cyclones) are also shifted further north, causing precipitation over the south and southeast regions (Reboita et al. 2010). So, the precipitation changes found here may result from a weakening of the SPSH denoted here by the easterly wind anomalies (between 30°S and 45°S) and by the poleward shift of the westerlies (south of 50°S) (Figure 5d-f). The trigger for the changes to the South American precipitation regime during the winter arises from the synchronous opposite response of the mean flow of the Pacific and Atlantic sectors. The maximum extremes of ASI lead to the positive phase of SAM (Pezza et al. 2012, Parise et al. 2015). Considering the entire simulation period (June 2020–July 2030), Parise et al. (2015) have found a decrease in the mean sea level pressure in high-latitudes (~ 3 hPa) and an increase in mid-latitudes (~ 1.5 hPa), being the response of this field most significant in southern autumn (MAM) and winter (JJA). By analyzing the response of South Atlantic tropospheric meridional circulation to increased coverage of ASI, Queiroz et al. (in press) have shown a signal inversion of the SAM, from the positive signal during the positive ASI phase (July 2020–June 2024) to the negative signal during the close to zero ASI phase (July 2024–June 2028). Queiroz et al. (in press) have also found a general cooling of the southern troposphere, from the surface to the upper levels, which led to a northward (southward) shift of the polar (subtropical) jet during the first four year of simulation (2020–2024), respectively. So, the strengthening (weakening) of the polar (subtropical) jet and the increased wind convergence at upper levels found here explain the reduced precipitation over south-central-north regions of Argentina (Figure 5d-f).

The most sensitive regions of South America continent to Antarctic sea ice positive extremes

Before analyzing the largest impacts of the ASI maxima on the precipitation over the six regions (R1 to R6) of South America, the Root Mean Square Error (RMSE) between the precipitation field from the CM2.1 model and ERA-Interim reanalysis was separately calculated (Figure 6a). The quarters with the best representation of the South American climate by the CM2.1 model were DJF, AMJ, MJJ and JJA. Among analyzed regions, the climate of Northwest of South America (R1) was the best represented by the model, with errors ranging from 0 to 1 mm in the first half of the year. In the Brazilian Amazon (North of Northeast), the lowest RMSE (0 to 2 mm) occurred in the second (first) half of the year, respectively. For the South of Northeast (R4), the RMSE ranged from 0.3 to 5.7 mm, with higher accuracy in AMJ and MJJ (RMSE from 0.3 to 0.7, respectively) and lower in JAS and ASO (RMSE from 4.9 to 5.7, respectively) quarters (Figure 6a). The Southeastern Brazil (R5) region showed RMSE values ranging from 0.7 to 3.8 mm, with MJJ showing the highest accuracy (RMSE of 0.7 mm) and the NDJ and JFM quarters showing the lowest accuracy (RMSE from 3.7 and 3.8 mm, respectively). The Southern Brazil (R6) region had the lowest RMSE (from 0.1 to 2.5 mm) in AMJ and SON, while the NDJ, JFM and MJJ quarters were those with most significant biases for this region (Figure 6a).

In order to analyze the climate scales with the largest impacts of the ASI maxima on the precipitation over the six regions of South

a)

Figure 6. a) Root of the Mean Square Error (RMSE) between the rainfall simulated by the CM2.1 model (*layerctl*) and the ERA-Interim reanalysis for the six regions with heterogeneous climate in South America: R1: Northwest of South America, R2: Brazilian Amazon, R3: North of Northeast Brazil, R4: South of Northeast Brazil, R5: Southeast Brazil and R6: South Brazil. Units are in mm day^{-1}; and **b)** Differences between the global power spectra of the *layermax* and *layerctl* ensemble experiments for each of the six regions with heterogeneous climate in South America (R1 to R6).

b)

America, the wavelet transform was applied on the *layermax-layerctl* differences field. The results have shown that the most extensive changes in the global potential spectrum between the analyzed series have occurred in the Brazilian Amazon (R2) (variance of 42 mm^2) and the Southeastern Brazil (R5) (variance of 20 mm^2) regions, especially in the interseasonal timescale (110 to 120 days) (Figure 6b). With the exception of R2, changes in higher frequency (~10 days) were also observed. In this timescale,

in general, there was a small decrease in spectral energy in Southern Brazil (R6) and a slight increase in other regions (Figure 6b).

As the most sensitive regions of the South American continent to the ASI positive extremes were the Brazilian Amazon (R2) and the Southeastern Brazil (R5) regions, the precipitation changes are also shown spatially for these regions (Figure 7). For R2, the greatest impacts occurred in spring (increased precipitation across the region) and summer
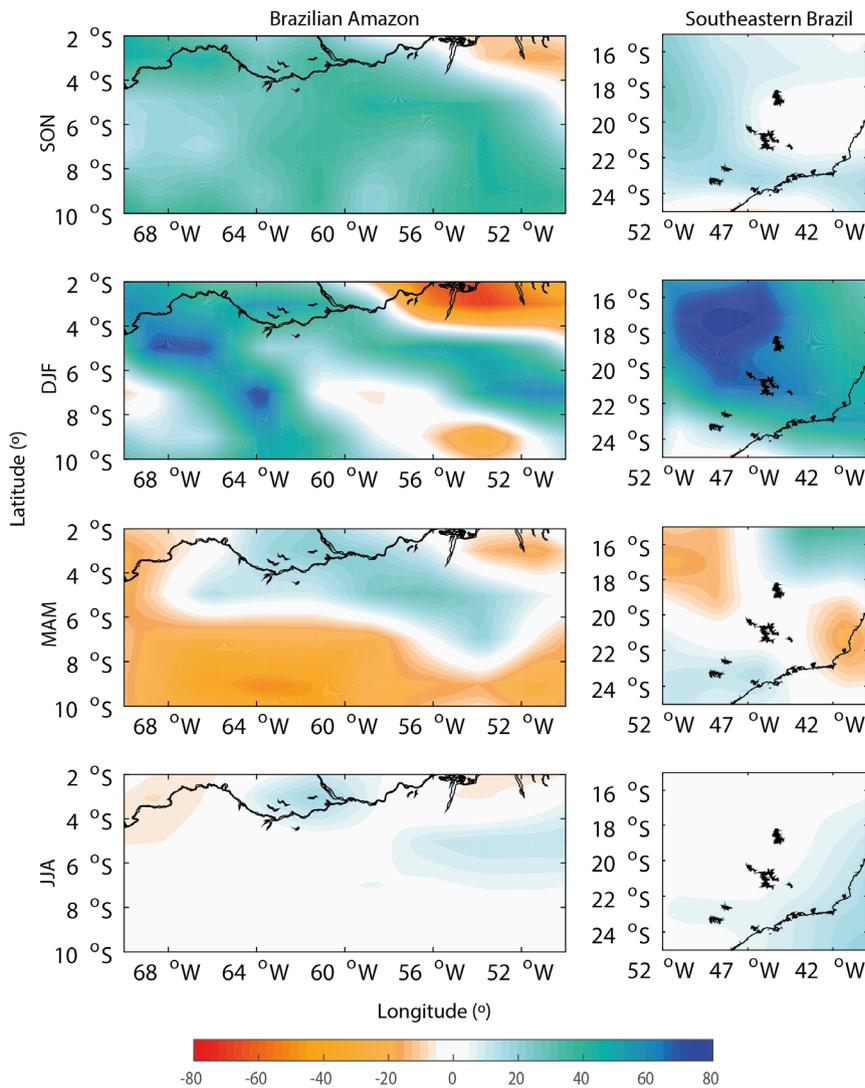
Figure 7. Spatial changes found for precipitation over the two regions most sensitive to the ASI positive extremes: the Brazilian Amazon (R2) and the Southeast Brazil (R5).

(decreased precipitation in some regions and increased in others, configuring a wave pattern 2). For R5, the greatest impacts occurred in summer, with increased precipitation (~80 mm season^{-1}) in the region (Figure 7).

DISCUSSION

Our discussion on the main changes found for the South American climate related to the ASI positive extremes is based on meteorological systems found here. The Northwest of South America (R1) region has great spatial heterogeneity in the precipitation field, being influenced by systems such as ITCZ, troughs, east waves, besides the regional and local effects such as the action of the easterly winds on the Andes topography that causes air convection over the mountains (Ramírez 2007). The precipitation in R1 is primarily influenced by Atlantic ITCZ and then by Pacific ITCZ. The last starts to operate in the region from September to October when the maximum precipitation peaks occur (Martelo 2003). An increase in precipitation over the R1 was observed by Carpenedo & Ambrizzi (2016) during extreme positive events of ASI due to

the intensification of the ascending branch of Hadley Cell and the consequent increase in the condensation of humid air by the trade winds in the ITCZ region. Here, the anomalous displacement of ITCZ to the north found in winter has resulted in reduced precipitation in R1.

The Brazilian Amazon (R2) has the highest total precipitation among the analyzed regions. The higher variance found in this region on the interseasonal timescale indicates that the maxima applied to ASI can also disturb the Madden-Julian Oscillation (MJO) through Walker's zonal circulation. In the fourth years since the imposing of ASI positive extremes (t_4), there was a strengthening of the SACZ during the spring, a period in which the South American Monsoon System typically starts, by increasing convective activity in the northeast of the Amazon basin (Vera et al. 2006, Silva & Kousky 2012), as well as in the summer. Saurral et al. (2014) observed an association between the ASI extent in the Weddell Sea and precipitation in South America, so that greater extent is associated with a strengthening of the SACZ and vice-versa. Changes in the position of ITCZ also influence precipitation in R2, especially in autumn (MAM), when the ITCZ is in its southernmost position (~2°S) (Melo et al. 2009).

The climate of Northeast Brazil presents heterogeneous spatial patterns of precipitation between its northern and southern sectors. In the North of Northeast Brazil (R3), the climatic maximum of precipitation occurs during the southern autumn (MAM) when the region is under the influence of ITCZ (Pezzi & Cavalcanti 2001). In addition, other mechanisms such as the UTCV formation in summer (t_4) and the Mesoscale Convective Complexes drive the variability of precipitation in R3 (Reboita et al. 2010). The interannual variability of precipitation in the Northeast Brazil occurs mainly due to

ENSO, a global phenomenon that also influences the precipitation in R3 through its atmospheric component (Walker Cell) and the Rossby wave trains (teleconnections), causing negative (El Niño) and positive (La Niña) anomalies of precipitation. In an extremely positive condition of observed ASI, Carpenedo & Ambrizzi (2016) showed that there was a surface cooling in the South Pacific Ocean and consequently the cooling of surface air, which has favored the occurrence of La Niña phase, bringing positive precipitation anomalies to the Northeast of Brazil. Pezza et al. (2012) have found a negative correlation between ENSO and ASI extent, that is, in La Niña years occurring with the positive phase of SAM would present the most favorable conditions for the general growth of ASI, except to the west of Antarctic Peninsula, where the opposite is seen. By analyzing the combined impacts of ENSO, SAM, and ASI on the cold fronts acting over the South America, Caldas et al. (2020) found that positive phase of ENSO and negative phase of SAM are associated to a maximum frequency of cold fronts for both minimum and maximum sea ice extensions in the Bellingshausen-Amundsen Sea (west of Antarctic Peninsula) and for maximum sea ice extensions in the Weddell Sea (east of Antarctic Peninsula).

In the South of Northeast Brazil (R4), the precipitation is influenced by synoptic systems that are frequently altered by large-scale circulation, such as the Walker Cell. Also, other systems that affect the precipitation in this region are the Bolivian High (although displaced to the east in relation to its climatological position), the Amazon moisture flows, the SACZ movement to the east and the southeast trade winds intensification (Chaves 1999).

The diversified climate of Southeastern Brazil (R5) is strongly dependent on its topography (Minuzzi & Sediyama 2005), where

SACZ (Rosa et al. 2020) and cold fronts appear as the main agents responsible for precipitation. These atmospheric systems acting together result in more intense SACZ events since the incursion of cold fronts in tropical latitudes reinforces the convective activity there (Nieto-Ferreira et al. 2011), as well as the transient systems, such as extratropical cyclones and cold fronts, provide the moisture supply to the SACZ region (Bombardi et al. 2014). In an opposite way, SASH and UTCV, depending on their positions, may cause long periods of drought in R5 (Minuzzi et al. 2007, Coelho et al. 2016). In the north of R5, there is a 3-months delay at the beginning of the rainy season in relation to the south, where it starts earlier according to the performance of the cold fronts (Alves et al. 2005). The SACZ greatest performance occurs in the summer (DJF), when the surface winds can transport greater amounts of moisture from the Amazon towards the Southwest Atlantic and, in some cases, producing the so-called Oceanic SACZ (Rosa et al. 2020), increasing the 95% percentile of daily precipitation in Southeastern Brazil (Carvalho et al. 2004). The spectral analysis performed here registered a peak of variance that started in December and extended until April (DJF, MAM) in the years simulated by the CM2.1 model, suggesting that the precipitation associated with SACZ was excited earlier and persisted for a longer time in response to the signal propagated from the Antarctic latitudes. This increase in the period of activity of SACZ was also documented by Silva (2018).

Any trend in SAM can have highly significant impacts on regional precipitation patterns (Gupta & England 2006). Excessive precipitation over Southeastern Brazil is associated with the positive phase of SAM (Vasconcellos & Cavalcanti 2010, Vasconcellos et al. 2019), which is related to positive extremes of ASI (Pezza et al. 2012, Parise et al. 2015). In the positive phase

of SAM (i.e., positive anomalies of mean sea level pressure in mid-latitudes), SASH tends to be positioned further south (Sun et al. 2017, Carpenedo & Ambrizzi 2020), influencing the strengthening of trade winds in some areas at south of northeast region of Brazil (Carpenedo & Ambrizzi 2020). Oppositely, in the negative phase of SAM, the SASH tends to be positioned further north, generating negative anomalies of precipitation in the north and northeast regions (Carpenedo & Ambrizzi 2020). Oliva et al. (2021), by examining the links between important teleconnection patterns (i.e., SAM; Atlantic Meridional Mode – AMM and South Atlantic Subtropical Gradient – SASG) to the Weddell Sea ice extent, have shown that the combinations between negative SAM and positive AMM as well as between negative SAM and positive SASG are associated to maximum Weddell Sea ice extent. The opposite combinations are associated with minimum Weddell Sea ice extent.

During the spring and summer, the performance of the low level jet was observed. The South America low level jet is a climatological feature with a critical role in the spatiotemporal distribution of precipitation in South America (Jones 2019). The low level jet can exceed $10\,\mathrm{m\,s^{-1}}$ in its northern branch from September to February. The northern branch is forced by a large-scale circulation pattern with the enhancement of the North Atlantic Subtropical High driving northeasterly winds over the northern Andes. The frequency and intensity of the low level jet in the northern Andes has substantially increased in the last 39 years (Jones 2019). When the low level jet is active only in the northern branch, wind speeds are very low from Bolivia towards SESA and precipitation is significantly reduced from climatology. In contrast, precipitation increases over eastern Bolivia.

Southern Brazil (R6) has a zonal spatial distribution, mainly due to factors related to its geographical position, presenting throughout the annual cycle, a monsoon regime to the north and maximum precipitation to the south (Grimm et al. 1998). Meteorological systems such as the breeze circulation (Braga & Krusche 2000), cold fronts (Andrade 2007), Mesoscale Convective Complexes (Durkee et al. 2009) and extratropical cyclones (Satyamurty & Mattos 1989) are very active in R6. For a positive ASI condition, the greater performance of extratropical cyclones was observed over the South Atlantic Ocean (Parise 2014), with significant impacts on the R6 climate (Carpenedo 2012). For this author, an increase in the sea ice extent in the Bellingshausen-Amundsen Seas is followed, three days later, by a drop (an increase) in air temperature in the south (southeast and northeast) regions of Brazil.

CONCLUSIONS

In this study, we analyzed the ability of the CM2.1 model on simulating the South American climate and its sensitivity to positive extremes, in area and volume, of ASI. The mechanisms of Pole-Equator teleconnections active in the transfer and dissipation of the climatic signal generated from high southern latitudes were also discussed. The seasonal changes in the South American climate were evaluated with the focus on the region with the highest precipitation and on atmospheric systems operating in each season. Our results show that the ASI positive extremes affect the South American climate, causing significant changes in the seasonal regime of precipitation, air temperature, and humidity driven by wind circulation changes at the lower and upper levels, as detailed below.

During the spring, the main changes caused by ASI positive extremes were: *i)* the gradual establishment of a SACZ pattern (an orientated northwest-southeast convective band acting over the SESA region and Southern-Southeastern Brazil); *ii)* cold and dry air biases and reduced precipitation over the north and northeast Brazil and later over the north of Argentina; *iii)* cyclonic circulation anomaly associated to wind convergence at low levels contributed to increasing the precipitation over Southeastern Brazil; *iv)* the UTCV formation and the Bolivian High strengthening and eastward shift were excited and pointed as two factors that carry precipitation to the central and northeast regions.

For the summer, the main changes observed were: *i)* a gradual establishment of a SACZ pattern in 925hPa air temperature occurred in a northwest-southeast oriented band over the south and central regions of Argentina and Southern and Southeastern Brazil; *ii)* cold and dry air is found over the north and northeast Brazil and later over the north of Argentina, both associated with reduced precipitation; *iii)* a low levels cyclonic circulation has contributed to wind convergence and increased precipitation over Southeastern Brazil; *iv)* the UTCV formation and the Bolivian High strengthening were excited and pointed as two factors that carry out precipitation to the region.

During the autumn, the ASI maxima were able to cause: *i)* changes in the ITCZ position; *ii)* negative air temperature anomalies over Southern Brazil associated with enhanced precipitation and low levels cyclonic circulation over the adjacent oceanic region; *iii)* the development of an upper levels anticyclonic circulation associated with less precipitation throughout the south and central regions of South America; *iv)* warmer and drier air masses over Southern Brazil indicating there were not the action of cold fronts; *v)* increased precipitation and humidity over Southeastern Brazil and

Paraguay, Bolivia, Northern Chile, Southern Peru and Eastern Pacific regions were associated with northwest wind anomalies converging from Peru and northwestern Brazil.

The main impacts of the ASI extremes on the South American climate during winter were: *i)* reduced precipitation over the Equatorial Atlantic, indicating a northward shift of ITCZ; *ii)* a northwest-southeast oriented band of reduced precipitation is associated with a low levels anticyclonic circulation at the east of Argentina; *iii)* reduced precipitation is found over Paraguay, the central region of Argentina and south, southeast and east regions of Brazil; *iv)* the weakening (strengthening) of the subtropical jet (polar jet) and the increased wind convergence at upper levels resulted in reduced precipitation over Paraguay and central region of Argentina.

The spectral analysis carried out in this study revealed that the periods with the greatest variance of the climatic signal resulting from disturbances applied on high southern latitudes occurred on the interseasonal timescale (110–120 days), especially over the Brazilian Amazon and the Southeastern Brazil regions.

The greater sensitivity of these two regions to the ASI positive extremes is directly related to the formation of a SACZ pattern, which proved to be highly sensitive to the signal generated from the Antarctic perturbation. Last, there are other factors in the coupled climate system, such as changes to the storm tracks and planetary waves that might complement the response of the South American climate to ASI positive extremes. These are interesting scientific subjects that are already under investigation and will be included in future publications.

Acknowledgments

REFERENCES

ADLER RF ET AL. 2003. The version-2 global precipitation climatology project GPCP monthly precipitation analysis (1979–Present). J Hydrometeorol 6: 1147-1167.

ALVES LM, MARENGO JA, CAMARGO JRH & CASTRO C. 2005. Início da estação chuvosa na região Sudeste do Brasil: Parte 1 - Estudos Observacionais. Rev Bras Meteor 3: 385-394.

ANDRADE KM. 2007. Climatologia e Comportamento dos Sistemas Frontais sobre a América do Sul. Dissertação de Mestrado em Meteorologia, INPE-14056-TDI/1067. (Unpublished).

BRAGA MFS & KRUSCHE N. 2000. Padrão de Ventos em Rio Grande, RS, no período de 1992 a 1995. Revista Atlântica 22: 27-40.

BINTANJA R, VAN OLDENBORGH GJ, DRIJFHOUT SS, WOUTERS B & KATSMAN CA. 2013. Important role for ocean warming and increased ice-shelf melt in Antarctic sea ice expansion. Nat Geosci 6: 376-379.

BITZ CM & POLVANI LM. 2012. Antarctic climate response to stratospheric ozone depletion in a fine resolution ocean climate model. Geophys Res Lett 39: L20705.

BOMBARDI RJ, CARVALHO LMV, JONES C & REBOITA MS. 2014. Precipitation over eastern South America and the South Atlantic Sea surface temperature during neutral ENSO periods. Clim Dyn 42: 1553-1568.

BUDD W, GORDON A, HEMPEL G, LORIUS C & WELLER G. 1989. The role of Antarctica in global change. Polar Record,

Prepared by the Steering Committee for the IGBP. ICSU Press/SCAR, Cambridge, p. 28.

CALDAS CF, VASCONCELLOS FC, CAVALCANTI IFA, CARVALHO NO & LOPES IR. 2020. Impacto do Gelo Marinho Antártico, do ENOS e do Modo Anular Sul sobre as Frentes Frias na América do Sul. Anuário do Instituto de Geociências - UFRJ. 43. 10.11137/2020_4_229_237.

CARPENEDO CB. 2012. Interações entre os ciclones extratropicais e a variabilidade extrema do gelo marinho nos mares de Bellingshausen-Amundsen e no mar de Weddell, Antártica. São Paulo: USP, 152 p.

CARPENEDO CB & AMBRIZZI T. 2016. Células de Circulação Meridional Durante os Eventos Extremos de Gelo Marinho Antártico. Rev Bras Meteorol, p. 251-0261.

CARPENEDO CB & AMBRIZZI T. 2020. Anticiclone Subtropical do Atlântico Sul Associado ao Modo Anular Sul e Impactos Climáticos no Brasil. Rev Bras Meteorol 35(4): 605-613.

CARPENEDO CB, AMBRIZZI T & AIMOLA LAL. 2013. Possíveis relações entre a variabilidade interanual do gelo marinho antártico e a precipitação na América do Sul. Ciênc Nat, p. 072-074.

CARVALHO LMV, JONES C & LIEBMANN B. 2004. The South Atlantic Convergence Zone: Intensity, Form, Persistence, and Relationships with Intraseasonal to Interannual Activity and Extreme Rainfall. J Clim 17: 88-108.

CAVALCANTI IFA & AMBRIZZI T. 2009. Teleconexões e suas influências no Brasil. In: CAVALCANTI IFA, FERREIRA NJ, SILVA MGAJ & DIAS MAFS (Orgs). Tempo e Clima no Brasil, São Paulo. Oficina de Textos, p. 317-335.

CAVALIERI DJ, PARKINSON CL, GLOERSEN P, COMISO JC & ZWALLY HJ. 1999. Deriving long-term time series of sea ice cover from satellite passive-microwave multisensor data sets. J of Geophys Res: Oceans 104(C7): 15803-15814.

CHAVES RR. 1999. Variabilidade da precipitação na região Sul do Nordeste e sua associação com padrões atmosféricos. São José dos Campos: INPE, p. 159.

COELHO CAS ET AL. 2016. The 2014 southeast Brazil austral summer drought: regional scale mechanisms and teleconnections. Clim Dyn 46: 1-16.

CUNNINGHAM CA & BONATTI JP. 2011. Local and remote responses to opposite ross sea ice anomalies: a numerical experiment with the CPTEC/INPE AGCM. Theor Appl Climatol, Springer Vienna 1-2: 23-44.

DEE DP ET AL. 2011. The ERA-Interim reanalysis: configuration and performance of the data assimilation system. Q J R Meteorol Soc 137: 553-597.

DELWORTH TL ET AL. 2006. GFDL's CM2 Global Coupled Climate Models. Part I: Formulation and Simulation Characteristics. J Clim 19: 643-674.

DURKEE JD, MOTE TL & SHEPHERD JM. 2009. The contribution of mesoscale convective complexes to rainfall across subtropical South America. J Clim 22: 4590-4605.

GILLETT NP, KELL TD & JONES PD. 2006. Regional climate impacts of the Southern Annular Mode. Geophys Res Lett 33(23): 1-4.

GOOSSE H, LEFEBVRE W, MONTETY A DE, CRESPIN E & ORSI OA. 2009. Consistent past half-century trends in the atmosphere, the sea ice, and the ocean at high southern latitudes. Clim Dyn 33: 999-1016.

GRIMM AM & AMBRIZZI T. 2009. Teleconnections into South America from the Tropics and Extratropics on Interannual and Intraseasonal Timescales. In: VIMEUX F, SYLVESTRE F & MYRIAM KHODRI (Orgs). Past Climate Variability in South America and Surrounding Regions. 1st ed., Springer Netherlands 14: 159-193.

GRIMM AM, FERRAZ SET & GOMES J. 1998. Precipitation anomalies in Southern Brazil associated with El Nihio and La Nifiaevents. J Clim 11: 2863-2880.

HOLLAND PR & KWOK R. 2012. Wind-driven trends in Antarctic sea-ice drift. Nat Geosci 5: 872-875.

JONES C. 2019. Recent changes in the South America low level jet. npj Clim Atmos Sci 2: 1-8. https://doi.org/10.1038/s41612-019-0077-5.

JONES C & CARVALHO LMV. 2002. Active and break phases in the South America monsoon system. J Clim 15: 905-914.

JONES DA & SIMMONDS I. 1993. A climatology of Southern Hemisphere extratropical cyclones. Clim Dyn 9: 131-145.

KOUSKY VE & GAN MA. 1981. Upper tropospheric cyclonic vortices in the subtropical South Atlantic. Tellus 33: 538-551.

LENTERS JD & COOK KH. 1997. On the Origin of the Bolivian High and Related Circulation Features of the South American Climate. J Atmos Sci 54(5): 656-678.

MANTA G, DE MELLO S, TRINCHIN R, BADAGIAN J & BARREIRO M. 2018. The 2017 record marine heatwave in the Southwestern Atlantic shelf. Geophys Res Let 45(12): 449.456.

MARTELO M. 2003. La precipitación en Venezuela y su relación con el sistema climático, Caracas, MARN, p. 72.

MENDELSOHN R, DINAR A & WILLIAMS L. 2006. The Distributional Impact of Climate Change on Rich and Poor Countries. Environ Dev Econ 11: 159-178.

MEEHL GA, ARBLASTER JM, BITZ CM, CHUNG CTY & TANG H. 2016. Antarctic sea-ice expansion between 2000 and 2014 driven by tropical Pacific decadal climate variability. Nat Geosci 9: 590-595.

MELO ABC, CAVALCANTI IFA & SOUZA PP. 2009. Zona de Convergência Intertropical do Atlântico. In: CAVALCANTI IFA, FERREIRA NJ, JUSTI DA SILVA MGA & SILVA DIAS MAF (Orgs). Tempo e Clima no Brasil. São Paulo: Oficina de Textos, cap. 2, p. 25-41.

MINUZZI RB & SEDIYAMA GC. 2005. Variabilidade do período chuvoso em regiões de alta e baixa altitudes. In: Conferência Regional sobre Mudanças Globais: América do Sul, 2, 2005, São Paulo. Anais. São Paulo: IEA, 2005. 1 CD-ROM.

MINUZZI RB, SEDIYAMA GC, BARBOSA EM & JÚNIOR JCFM. 2007. Climatologia do comportamento do período chuvoso da região sudeste do Brasil. Rev Bras Meteorol 3: 338-344.

NIETO-FERREIRA R, RICKENBACH TM & WRIGHT EA. 2011. The role of cold fronts in the onset of the monsoon season in the South Atlantic convergence zone. Q J R Meteorol Soc 137(657): 908-922.

NOAA/NCDC. 2014: State of the climate: Global snow and ice for September 2013. Accessed 19 August 2014. [Available online at http://www.ncdc.noaa.gov/sotc/global-snow/201309.].

OLIVA FG, VASCONCELLOS FC, SILVA TM & PIZZOCHERO RM. 2021. Extremos de Gelo Marinho Antártico no Mar de Weddell e Relações com Padrões de Teleconexões Climáticas. Rev Rev Bras Geof Fis 14: 2739-2754.

PARISE CK. 2014. Sensitivity and memory of the current mean climate to increased Antarctic sea ice: The role of sea ice dynamics, São José dos Campos: INPE, p. 218.

PARISE CK, PEZZI LP, HODGES KI & JUSTINO F. 2015. The influence of sea ice dynamics on the climate sensitivity and memory to increased Antarctic sea ice. J Clim 28: 9642-9668.

PARKINSON CL. 2019. A 40-y record reveals gradual Antarctic sea ice increases followed by decreases at rates far exceeding the rates seen in the Arctic. P Natl Acad Sci USA 116: 14414-14423.

PEZZA AB, RASHID HA & SIMMONDS I. 2012. Climate links and recent extremes in Antarctic sea ice, high-latitude cyclones, southern annular mode and ENSO. Clim Dyn 38(1-2): 57-73.

PEZZI LP & CAVALCANTI IFA. 2001. The relative importance of ENSO and tropical Atlantic sea surface temperature anomalies for seasonal precipitation over South America: a numerical study. Clim Dyn 17(2-3): 205-212.

PEZZI LP & KAYANO MT. 2008. An analysis of the seasonal precipitation forecasts in South America using wavelets. J Clim 29: 1560-1573.

PEZZI LP, QUADRO MFL, LORENZZETTI JA, MILLER AJ, ROSA EB, LIMA LN & SUTIL UA. 2022. The effect of Oceanic South Atlantic Convergence Zone episodes on regional SST anomalies: the roles of heat fluxes and upper-ocean dynamics. Clim Dyn. https://doi.org/10.1007/s00382-022-06195-3.

POLVANI LM, WAUGH DW, CORREA GJP & SON SW. 2011. Stratospheric ozone depletion: The main driver of twentieth century atmospheric circulation changes in the Southern Hemisphere. J Clim 24: 795-812.

RAMÍREZ JGM. 2007. Estudo de sistemas convectivos na Venezuela por meio de sensoriamento remoto com satélite, São Paulo: USP, p. 78.

RAPHAEL M, HOBBS W & WAINER I. 2011. The effect of Antarctic sea ice on the southern hemisphere atmosphere during the southern summer. Clim Dyn 7-8: 1403-1417.

RATISBONA LR. 1976. The Climate of Brazil: Climate of Central and South America. In World Survey of Climatology, Chap 5, SCHWERDTFEGER W & LANDSBERG HE (Eds). Elsevier: Amsterdam 12: 219-293.

RAYNER NA, PARKER DE, HORTON EB, FOLLAND CK, ALEXANDER LV, ROWELL DP, KENT EC & KAPLAN A. 2003. Global analyses of sea surface temperature, sea ice, and night marine air temperature since the late nineteenth century. J Geophys Res 108(D14): 4407. doi:10.1029/2002JD002670.

REBOITA MS, GAN MA, DA ROCHA RP & AMBRIZZI T. 2010. Regimes de Precipitação na América do Sul: Uma Revisão Bibliográfica. Rev Bras Meteorol 25: 185-204.

ROSA EB, PEZZI LP, QUADRO MFLD & BRUNSELL N. 2020. Automated Detection Algorithm for SACZ, Oceanic SACZ, and Their Climatological Features. Front Environ Sci 8: 18.

SATYAMURTY P & MATTOS LF. 1989. Climatological lower tropospheric frontogenesis in the midlatitudes due to horizontal deformation and divergence. Mon Weather Rev 117(6): 1355-1364.

SAURRAL R, BARROS V & CAMILLONI I. 2014. Sea ice concentration variability over the Southern Ocean and its impact on precipitation in southeastern South America. Int J Climatol 34: 2362-2377.

SILVA RC. 2018. Eventos Extremos de Gelo Marinho no Mar de Weddell e sua relação com o Anticiclone Subtropical do Atlântico Sul, Uberlândia: UFU, p. 70.

SILVA VBS & KOUSKY VE. 2012. The South American Monsoon System: Climatology and Variability, Modern Climatology, Dr Shih-Yu Wang (Ed), InTech.

SIMMONDS I, KEAY K & LIM EP. 2003. Synoptic activity in the seas around Antarctica. Mon Weather Rev 131: 272-288.

SINCLAIR MR. 1994. An objective cyclone climatology for the Southern Hemisphere. Mon Weather Rev 122: 2239-2256.

SIGMOND M & FYFE JC. 2010. Has the ozone hole contributed to increased Antarctic sea ice extent? Geophys Res Lett 37: L18502.

STAMMERJOHN SE, MARTINSON DG, SMITH RC, YUAN X & RIND D. 2008. Trends in Antarctic annual sea ice retreat and advance and their relation to El Niño–Southern Oscillation and southern annular mode variability. J Geophys Res 113: C03S90.

SUN X, COOK KH & VIZY EK. 2017. The South Atlantic subtropical high: climatology and interannual variability. J Clim 30: 3279-3296.

SWART NC & FYFE JC. 2013. The influence of recent Antarctic ice sheet retreat on simulated sea ice area trends. Geophys Res Lett 40: 4328-4332.

TAYLOR K, WILLIAMSON D & ZWIERS F. 2000. The Sea Surface Temperature and Sea-ice Concentration Boundary Conditions for AMIP II Simulations. PCMDI, p. 28.

THOMPSON DWJ & SOLOMON S. 2002. Interpretation of recent Southern Hemisphere climate change. Science 296: 895-899.

THOMPSON DWJ, SOLOMON S, KUSHNER PJ, ENGLAND MH, GRISE KM & KAROLY DJ. 2011. Signatures of the Antarctic ozone hole in Southern Hemisphere surface climate change. Nat Geosci 4: 741-749.

THOMPSON DWJ & WALLACE JM. 2000. Annular modes in the extratropical circulation. Part I: Month-to-month variability. J Clim 13(5): 1000-1016.

TURNER J ET AL. 2020. Recent decrease of summer sea ice in the Weddell Sea, Antarctica. Geophys Res Lett 47: e2020GL087127.

TURNER J, HOSKING JS, BRACEGIRDLE TJ, MARSHALL GJ & PHILLIPS T. 2015. Recent changes in Antarctic sea ice. Philos Trans R Soc A Math Phys Eng Sci Vol. 373.https://doi.org/10.1098/rsta.2014.0163.

TURNER J & OVERLAND J. 2009. Contrasting climate change in the two polar regions. Polar Res 28: 146-164.

TURNER J ET AL. 2009. Non-annular atmospheric circulation change induced by stratospheric ozone depletion and its role in the recent increase of Antarctic sea ice extent. Geophys Res Lett 36: L08502.

VASCONCELLOS FC & CAVALCANTI IFA. 2010. Extreme precipitation over Southeastern Brazil in the austral summer and relations with the Southern Hemisphere annular mode. Atmosph Sci Lett 11: 21-26.

VASCONCELLOS FC, PIZZOCHERO R & CAVALCANTI I. 2019. Month-to-Month Impacts of Southern Annular Mode Over South America Climate. Anuário do Instituto de Geociências 42(1): 783-792.

VELEDA D, MONTAGNE R & ARAUJO M. 2012. Cross-Wavelet Bias Corrected by Normalizing Scales. J Atmos Ocean Technol 29: 1401-1408.

VERA C ET AL. 2006. Towards a unified view of the American Monsoon systems. J Clim 19: 4977-5000.

ZHANG J. 2007. Increasing Antarctic sea ice under warming atmospheric and oceanic conditions. J Clim 20: 2515-2529.

ZHOU J & LAU KM. 1998. Does a monsoon climate exist over South America? J of Clim 11: 1020-1040.

SUPPLEMENTARY MATERIAL

Figure S1. Seasonal mean precipitation rate (colors, in mm day^{-1},), 925hPa wind (vectors, in ms^{-1}) and 200hPa wind in ms^{-1}(stream lines) simulated over the South American continent by the *layerctl* ensemble experiment during the first 4-years: a) Spring (SON), b) Summer (DJF), c) Autumn (MAM) and d) Winter (JJA).
Figure S2. Cross-section of the zonal mean zonal wind during spring (SON), summer (DJF), autumn (MAM), winter (JJA): left column) CM2.1 model (*layerctl*) and right column) ERA-Interim Reanalysis (1979–2020).
Figure S3. Wavelet spectral analysis of precipitation at each of the six regions with heterogeneous climate in South America (R1 to R6) provided by ERA-Interim reanalysis (2017–2020).
Figure S4. Wavelet Spectral analysis of precipitation at each of the six regions with heterogeneous climate in South America (R1 to R6) provided for the *layerctl* ensemble mean (2020–2024).

CLÁUDIA K. PARISE[1]
https://orcid.org/0000-0002-9466-788X

LUCIANO P. PEZZI[2]
https://orcid.org/0000-0001-6016-4320

CAMILA B. CARPENEDO[3]
https://orcid.org/0000-0001-9034-789X

FERNANDA C. VASCONCELLOS[4]
https://orcid.org/0000-0002-5931-1503

WESLEY L. BARBOSA[1]
https://orcid.org/0000-0002-9279-5626

LEONARDO G. DE LIMA[5]
https://orcid.org/0000-0001-7449-8639

[1]Universidade Federal do Maranhão (UFMA), Departamento de Oceanografia e Limnologia (DEOLI), Laboratório de Estudos e Modelagem Climática (LACLIMA), Avenida dos Portugueses, 1966, Vila Bacanga, 65080-805 São Luís, MA, Brazil

[2]Instituto Nacional de Pesquisas Espaciais (INPE), Divisão de Observação da Terra e Geoinformática (DIOTG), Laboratório de Estudos do Oceano e da Atmosfera (LOA), Avenida dos Astronautas, 1758, Jardim da Granja, 12227-010 São José dos Campos, SP, Brazil

[3]Universidade Federal do Paraná (UFPR), Departamento de Solos e Engenharia Agrícola (DSEA), Rua dos Funcionários, 1540, Cabral, 80035-050 Curitiba, PR, Brazil

[4]Universidade Federal do Rio de Janeiro (UFRJ), Departamento de Meteorologia, Avenida Athos da Silveira Ramos, 274, Cidade Universitária, 21941-916 Rio de Janeiro, RJ, Brazil

[5]Universidade Federal do Maranhão (UFMA), Departamento de Oceanografia e Limnologia (DEOLI), Laboratório de Estudos de Oceanografia Geológica (LEOG), Avenida dos Portugueses, 1966, Vila Bacanga, 65080-805 São Luís, MA, Brazil

Correspondence to: **Cláudia Klose Parise**
E-mail: claudiakparise@gmail.com

Author contributions

Cláudia K. Parise has carried out the sensitivity ensemble experiments, performed all the data treatment and analysis and wrote the manuscript. Luciano P. Pezzi has contributed with the infrastructure needed for carrying out the numerical experiments and helped to write the manuscript. Camila B. Carpenedo and Fernanda C. Vasconcellos helped to discuss the results found. Wesley L. Barbosa has performed the spectral analyses for the South America regions. Leonardo G. de Lima helped to discuss the results found and also contributed to creation and consolidation of the Laboratory for Climate Studies and Modelling (LaClima) at the Department of Limnology and Oceanography of Federal University of Maranhão Where most analyzes were conducted.